J. Fluid Mech. (2006), *vol.* 553, *pp.* 75–84. © 2006 Cambridge University Press
doi:10.1017/S0022112006009013 Printed in the United Kingdom

Jetting–dripping transition of a liquid jet in a lower viscosity co-flowing immiscible liquid: the minimum flow rate in flow focusing

By ALFONSO M. GAÑÁN-CALVO
AND PASCUAL RIESCO-CHUECA

E.S.I., Universidad de Sevilla, Camino de los Descubrimientos s/n 41092 Seville, Spain

(Received 3 November 2005 and in revised form 14 January 2006)

We study the jetting–dripping (J–D) transition of a flow-focused viscous liquid jet surrounded by a co-flowing immiscible, lower viscosity liquid. A theoretical model describing wave propagation in open cylindrical flows has been adapted to our problem and further expanded to incorporate spatio-temporal stability considerations (global modes). The J–D transition sets the minimum liquid flow rate issuing as a steady jet and breaking up into droplets whose size is commensurate with the jet diameter. At the onset of dripping, droplets become considerably larger than jetting droplets, under comparable flow parameters. A linear theory accounting for convective and absolute instability is provided, along with a detailed interpretation of the parametrical space, under realistic viscosity and density restrictions. The experimental part sums up a collection of laboratory data illustrating the J–D transition with good agreement with the theory.

1. Introduction

The hydrodynamic stability theory of spatially developing flows was surveyed by Huerre & Monkewitz (1990), with respect to the space and time development of infinitesimal perturbations around a given basic flow. Open shear flows (mixing layers, jets, wakes, boundary layers) have provided evidence that strictly local and spatial instability theory (real frequency) may not be generally appropriate. Wavenumber and frequency both need to be considered complex, opening the door to absolute/convective (C/A) and local/global instability concepts. However, the complexity of such formulations has limited all analytic studies so far to relatively simple flow patterns. In our case, the theory for C/A instability of liquid jets is burdened by algebraic difficulties, which have been addressed by drastic simplifications. The seminal study on the temporal instability of jets by Rayleigh (1878), the spatial instability analysis of Keller, Rubinow & Tu (1973), and the study of C/A instability by Leib & Goldstein (1986*b*) neglect viscosity and other ambient effects. Leib & Goldstein (1986*a*, *b*) incorporate the jet viscosity but neglect the ambient. Below a given critical Weber number, of order unity, the Rayleigh instability is replaced by an absolute instability. The Weber number being defined as $We = \rho V^2 R_j \sigma^{-1}$ (ρ is the jet density, and V, R_j its speed and radius), this amounts to capillary forces becoming comparable to inertia forces. An overview of the progress in this field is summarized by Ashgriz & Mashayek (1995).

Several studies on the J–D transition appear to strengthen the causal link with the onset of absolute instability (Lin & Lian 1989; Monkewitz *et al.* 1988; Monkewitz

1990; Lin & Lian 1993; Clanet & Lasheras 1999). O'Donnell, Chen & Lin (2001) provide experimental evidence of the C/A transition at relatively large Reynolds numbers: when the ratio of the surface energy to the kinetic energy per unit length of the jet is sufficiently large, the disturbance can propagate and amplify both in the downstream and upstream directions (absolute instability); when this ratio is small, the disturbance can only propagate and amplify in the downstream direction (convective instability). In Le Dizes (1997), the global linear stability analysis of falling capillary jets neglects the viscosity and the density of the ambient gas; beyond a critical Weber, the basic flow is convectively unstable everywhere except at the orifice where the instability is absolute. Other examples of the transition in the breakup of sheets and jets are presented by Lin (2003); the C/A transition goes hand in hand with the J–D transition under gravity. However, experimental evidence is clouded by several phenomena that interfer. The experiments by Monkewitz *et al.* (1988), measuring the breakup distance between the jet origin and the first-drop location, cover a wide range of Weber and Reynolds numbers. As a critical Weber number is reached, the breakup distance is observed to decrease suddenly; eventually, it becomes zero if *We* is further reduced. At this critical Weber number the jet evolves from breaking up at a downstream location to dripping, while the mean flow rate remains substantially invariant. The authors explain this behaviour by assuming an absolute instability region to develop next to the orifice; the resulting finite-amplitude oscillations probably lead to the wetting of the nozzle and to the formation of large drops. Cramer, Fischer & Windhab (2004) explore drop formation at a capillary tip in laminar flow. The dispersed phase is injected via a needle into a co-flowing immiscible fluid. Jetting becomes more probable with increasing velocity of the continuous phase, higher flow rate and viscosity of the dispersed phase and lower interfacial tension. All parameters enhancing the ambient drag force and increasing the momentum of the disperse phase favour the generation of a liquid jet.

It is our goal to contribute some insight (both experimental and theoretical) into the J–D transition of viscous jets under the influence of a viscous ambient. We draw on previous studies on the stability of coaxial flows. A common limitation to all theoretical endeavours is their analytical complexity; on the other hand, experiments are complicated by the simultaneous influence of diverse instability sources, and by the taxonomic diversity of breakup. This leads to some interpretative difficulties, among them the existence of combined instability phenomena caused by the interference of local and global sources. Lin & Lian (1993) study the C/A instability of a viscous liquid jet emanating into a viscous gas in a vertical pipe. The domain of absolute instability is significantly enlarged when the effect of gas viscosity is not neglected. Funada & Joseph (2002) generalize the inviscid analysis of Rayleigh (1878) by accounting for the viscosity of the jet and for the viscosity and density of the ambient. A stream function for both phases leads to a dispersion relation for fully viscous fluids, but a spatio-temporal analysis is not undertaken. Funada, Joseph & Yamashita (2004) use a simplified dispersion relation (assuming potential flow and limiting viscous effects to viscous stress at the interface) to describe C/A stability. Sevilla, Gordillo & Martinez-Bazan (2005) study inviscid coaxial air–water jets discharging into a stagnant air atmosphere assuming a piecewise-uniform basic velocity profile. Their analysis shows that the change from bubbling to jetting can be understood in terms of a C/A transition.

In the following, a fully viscous formulation as in Funada & Joseph (2002) will be explored using a linear, local, spatio-temporal theory; the breakup dynamics cannot be described with our linear theory, but the response to small perturbations

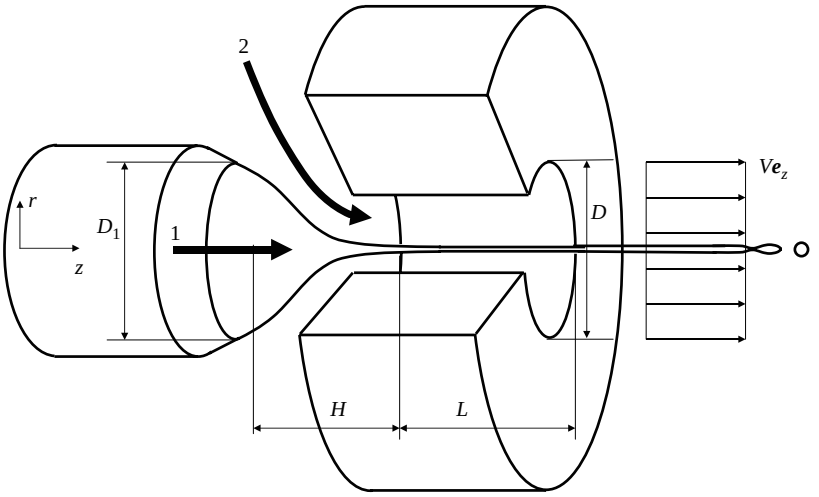

FIGURE 1. Flow-focusing setup: a nozzle emits a liquid filament 1, which is pulled by a pressurized co-flowing fluid 2; both phases are evacuated through a coaxial orifice.

is a helpful tool to predict breakup occurrence. To map the J–D transition, we track the evolution of the limit curve starting from the results by Leib & Goldstein (1986*b*); the curve is cautiously perturbed to explore effects of the ambient liquid. The analytical results will be tested using a compound oil–water jet produced by flow focusing.

2. Theoretical analysis

2.1. *The dispersion relation*

Consider the spatio-temporal stability of a core liquid jet produced by flow focusing (FF) (in figure 1, the core liquid 1 is surrounded by a shell of immiscible co-flowing liquid 2; liquid viscosities $\mu_{1,2}$ and densities $\rho_{1,2}$; cylindrical coordinates are r, z). The following assumptions hold. (i) Both liquids are viscous and immiscible; their interfacial surface tension is σ. (ii) The Reynolds number of the co-flowing shell $Re_2 = \rho_2 V D \mu_2^{-1}$ is large enough to ensure a uniform streamwise velocity $V\boldsymbol{e}_z$ around the liquid jet, $\boldsymbol{e}_z$ being the axial unit vector. (iii) The liquid jet diameter $d_j = 2R_j$ is roughly uniform and much smaller than the orifice diameter D, $d_j/D \ll 1$, so that the jet can be considered to flow in an unbounded co-flowing liquid domain moving with uniform velocity V; this simplification (both in the theory and in the setup) is an attempt to enforce cylindrical homogeneity. Our choice circumvents the complexity of a downstream variation of the flow regime (and hence, excludes the possibility of heterogeneous stability behaviour at different axial locations). We are thus considering purely cylindrical flow patterns, and disregarding the effects of local instability sources (e.g. oscillation of the meniscus). (iv) The axial length l required for a full momentum diffusion from the shell to the core, $l \sim \rho_1 V \mu_1^{-1} d_j^2$, is small compared to the axial length of the orifice L, $l/L \ll 1$, and thus both liquid streams move with a similar uniform axial velocity V. (v) No azimuthal modes are considered (pure axisymmetric motion), a simplification supported by extensive literature (see Lin & Webb 1994), both theoretical and experimental, on the J–D transition.

We analyse the system response under a perturbation wave $\exp[\mathrm{i}(kz - \Omega t)]$. The dispersion relation for a viscous liquid cylinder in an immiscible viscous ambient

liquid has been studied by Tomotika (1935), Funada & Joseph (2002) and Funada *et al.* (2004). Wave frequency Ω, time t, wavenumber k and coordinates $\{r, z\}$ are scaled with V/R_j, R_j/V, $1/R_j$ and R_j respectively. Four dimensionless parameters arise: the Reynolds and Weber numbers, and the liquid density and viscosity ratios:

$$Re = \rho_1 V R_j \mu_1^{-1},\ We = \rho_1 V^2 R_j \sigma^{-1},\ \alpha = \rho_2/\rho_1,\ \beta = \mu_2/\mu_1. \tag{2.1}$$

A dimensionless dispersion relation $S(\hat{\omega}, x; Re, We, \alpha, \beta) = 0$ (with $\hat{\omega} = R_j \Omega V^{-1}$ and $x = R_j k$) has been obtained by Funada & Joseph (2002) and fully simplified by us to

$$S \equiv \left(x^2 - y_1^2\right)\left[\frac{N(x, y_1, y_2, \beta)}{M(x, y_1, y_2, \beta)} + 2(1-\beta)\right] - \frac{Re^2}{We}(1 - x^2) = 0 \tag{2.2}$$

where 'viscous' wavenumbers are defined for both liquids as

$$y_1^2 = x^2 - \mathrm{i} Re\hat{\omega}, \quad y_2^2 = x^2 - \mathrm{i}\alpha\beta^{-1} Re\hat{\omega}, \tag{2.3}$$

and functions N and M are expressed as

$$\begin{aligned} N \equiv\ & 2x\beta y_1 y_2 \left[K_0(y_2) I_1(y_1) y_1 + I_0(y_1) K_1(y_2) y_2\right] \\ & + x\left[x^2(\beta - 1) - y_1^2 + \beta y_2^2\right]^2 I_0(x) I_1(y_1) K_0(x) K_1(y_2) \\ & + 4x^3 y_1 y_2 (\beta - 1)^2 I_0(y_1) I_1(x) K_0(y_2) K_1(x) \\ & - y_2 I_1(y_1) K_0(y_2)\left\{\left[x^4 + y_1^2 y_2^2 + x^2\left(y_1^2 - y_2^2\right)\right]\beta I_1(x) K_0(x)\right. \\ & \left. + \left[y_1^4 + x^4(1 - 2\beta)^2 - 2x^2 y_1^2(\beta - 1)\right] I_0(x) K_1(x)\right\} \\ & + y_1 I_0(y_1) K_1(y_2)\left\{\left[x^4(\beta - 2)^2 + 2x^2 y_2^2 \beta(\beta - 1) + \beta^2 y_2^4\right] I_1(x) K_0(x)\right. \\ & \left. + \left[x^2\left(x^2 - y_1^2\right) + y_2^2\left(x^2 + y_1^2\right)\right]\beta I_0(x) K_1(x)\right\}, \end{aligned} \tag{2.4}$$

$$\begin{aligned} M \equiv\ & x\left\{\left[y_2 K_0(y_2) K_1(x) - x K_0(x) K_1(y_2)\right]\left(y_1^2 - x^2\right) I_1(x) I_1(y_1)\right. \\ & \left. + \beta\left[y_1 I_0(y_1) I_1(x) - x I_0(x) I_1(y_1)\right]\left(y_2^2 - x^2\right) K_1(x) K_1(y_2)\right\}. \end{aligned} \tag{2.5}$$

Interestingly, the limit $\alpha \to 0$, $\beta \to 0$ yields

$$\frac{N}{M} \to \frac{\left(x^2 + y_1^2\right)^2}{x\left(x^2 - y_1^2\right)}\frac{I_0(x)}{I_1(x)} - \frac{4x^2 y_1}{\left(x^2 - y_1^2\right)}\frac{I_0(y_1)}{I_1(y_1)}. \tag{2.6}$$

This leads to the liquid–vacuum dispersion relation in Chandrasekhar (1961) and Leib & Goldstein (1986*a*) (we report here a new abridged expression for the same limit):

$$S \equiv \left(x^2 + y_1^2\right)^2 \frac{I_0(x)}{I_1(x)} - 4x^3 y_1 \frac{I_0(y_1)}{I_1(y_1)} + 2x\left(x^2 - y_1^2\right) + \frac{Re^2}{We} x(x^2 - 1) = 0. \tag{2.7}$$

Three key remarks are now introduced:

(i) To change the reference system from a travelling observer to a fixed observer anchored at the nozzle, we just need to replace the wave frequency $\Omega = V R_j^{-1}\hat{\omega}$ by $\Omega' = V R_j^{-1}(\omega - x)$ in the dispersion relation (Leib & Goldstein 1986*a*). The new ω is the dimensionless wave frequency for the static observer. This can be proved by retaining the linearized convective terms $V u_z$ and $V R_z$ in the momentum equation and the kinematic condition at the interface, respectively. In a fixed coordinate system, y_1 and y_2 are

$$y_1 = \pm\left[x^2 - \mathrm{i} Re(\omega - x)\right]^{1/2},\ y_2 = \pm\left[x^2 - \mathrm{i}\alpha\beta^{-1} Re(\omega - x)\right]^{1/2}. \tag{2.8}$$

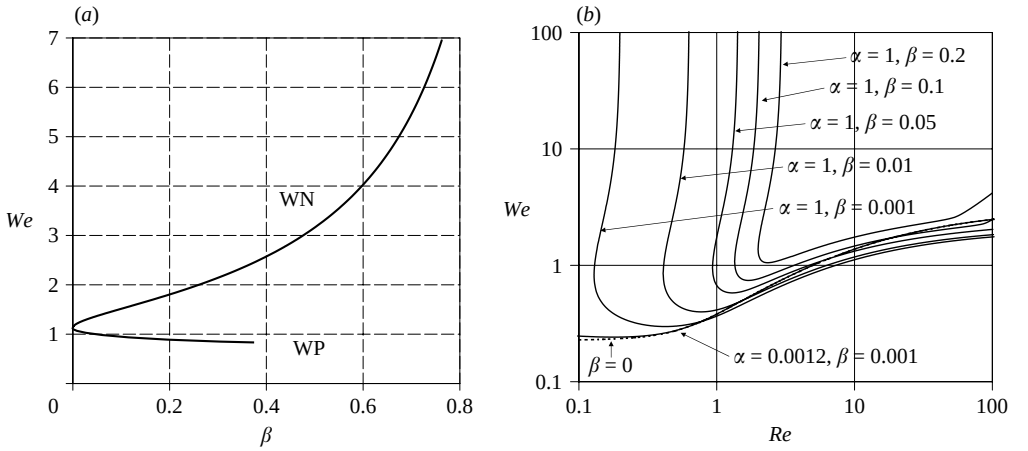

FIGURE 2. (*a*) J–D transition in the $\{\beta, We\}$-plane ($Re = 11.2$ and $\alpha = 1$). Two theoretical transition curves corresponding to positive (WP) and negative (WN) y_2 roots are plotted. (*b*) J–D transition in the $\{Re, We\}$-plane. The L-G limit is plotted as a dotted line.

(ii) Both ω and x are complex. Therefore, $\omega = \omega_r + \mathrm{i}\omega_i$ and $x = x_r + \mathrm{i}x_i$, $\{\omega_r, \omega_i, x_r, x_i\}$ being real numbers ('oscillation frequency', 'local growth rate', 'wavenumber' and 'spatial growth rate', respectively).

(iii) It follows that both roots of the viscous wavenumbers y_1 and y_2 must be explored in the analysis, to encompass all potential sources of spatio-temporal instability. The theoretical framework supporting the results in Funada & Joseph (2002) and Funada *et al.* (2004) does not require such a precaution. However, we observed the dispersion relation to be symmetric with respect to y_1, so that identical $\{\omega, x\}$ pairs result, no matter which root $\pm y_1$ is chosen. This is not the case with y_2, whose positive and negative roots yield completely different results, implying different wave solution pairs $\{\omega, x\}$.

With these remarks in mind, we carry out a spatio-temporal stability analysis (e.g. Leib & Goldstein 1986*a*, *b*; Huerre & Monkewitz 1990; Chomaz 2005) to map absolutely unstable wave conditions. These are confined to specific regions of the complete parametrical space $\{Re, We, \alpha, \beta\}$. It is our aim to attempt a *partial* exploration of this space: we will focus on the $\beta < 1$ range, with particular emphasis on the frequent microfluidic assumption $\alpha \simeq 1$, as in the atomization of a liquid polymer solution surrounded by water or any polar solvent.

2.2. *Analytical results*

Our dispersion relation can be easily reduced to the limit in Leib & Goldstein (1986*a*) (L-G limit) by setting $\beta = 0$. At this limit, there is a single wave solution, absolutely unstable, for both positive and negative roots of y_1^2. On moving away from this limit solution, under fixed Re and α (e.g. $Re = 11.2$; $\alpha = 1$), β is changed to evaluate the J–D transition loci. Two branches WP and WN are plotted in figure 2(*a*), associated with the positive and negative roots of y_2^2. Both solutions collapse when $\beta \to 0$. Interestingly, the WN-branch is the one that provides physically meaningful J–D loci $\{\beta, We\}$. Moving through on the $\{We, \beta\}$ space in figure 2(*a*) (from jetting towards dripping), we first cross the negative branch WN. Obviously, as we move deeper in the lower $\{Re, We\}$ region (smaller flow rates), we would eventually hit the second branch WP, but this is physically irrelevant since absolute instability modes

are already activated (leading to dripping) once the transition through the WP-branch has taken place. The formal procedure to determine the J–D loci is based (Huerre & Monkewitz 1990) on the simultaneous solution of the dispersion relation along with the constraint that the group velocity be zero. The resulting solutions $\{\omega^*, x^*\}$ happen to be saddle points; some further checks are required before identifying them as J–D transition points. In short, we look for points $\{\omega^*, x^*\}$ where $S=0$ and $\partial S/\partial x=0$, with $x_i^* < 0, \omega_i^* = 0$; in addition, the branches issuing from the saddle point should cross the real x-axis so as to define a range of unstable wavelengths. These conditions identify the associated parametrical point $\{Re^*, We^*, \alpha^*, \beta^*\}$ as being located at the boundary (i.e. $\omega_i^*=0$) of absolutely unstable behaviour.

Figure 2(*b*) shows several J–D transition lines separating the $\{Re, We\}$-plane into absolutely unstable (dripping) and convectively unstable (jetting) regions, for $\alpha=1$, $\alpha=1.03$ and various values of β. The L-G solution is represented as a dotted line. Observe that the J–D lines exhibit an elbow or fold which is not present in the L-G limit ($\beta=0$). Thus, dripping may be obtained by sufficiently depressing either *Re* or *We*. The plot also shows the L-G limit to closely fit our model when $\alpha=0.0012$ and $\beta=0.001$ (water jet in air). Note that the L-G model fails to describe low-*Re* situations, where the influence of the outer fluid cannot be ignored.

Steady micro-jetting gives rise to greater productivity (larger liquid flow rates), with a well-controlled and small drop size. On the contrary, dripping gives rise to much larger, isolated droplets under similar *Re* and *We*. Dripping usually yields a highly monodisperse spray, but it may also exhibit bi-disperse or polydisperse droplet distributions: see Coullet, Mahadevan & Riera (2005); an analogous phenomenon in flow-focusing micro-bubbling is described by Garstecki, Fuerstman & Whitesides (2005). Here we postulate that such nonlinear complex dynamics may arise whenever a given parametrical set $\{Re, We, \alpha, \beta\}$ leads to more than one absolutely unstable wave solution and these solutions exhibit similar local growth rate ω_i but different local oscillation frequency ω_r.

3. Experimental verification

A stainless steel FF device with dimensions $D=D_1=150\,\mu\text{m}$, $L=160\,\mu\text{m}$, and $H=125\,\mu\text{m}$ is used. The inner edge of the orifice has been rounded to minimize *vena contracta* effects. The ambient focusing fluid is distilled water at $T=23^\circ\text{C}$ ($\rho_2=995\,\text{kg m}^{-1}$, $\mu_2=0.001\,\text{Pa s}$). Three silicone oils with nominal Newtonian viscosities μ_1 equal to 0.005, 0.02 and 0.1 Pa s and measured oil–water surface tensions $\sigma=33.2$, 30.4, and $28\,\text{mN m}^{-1}$ at $T=23^\circ\text{C}$ are used as the jet-forming liquid. The oil densities are $\rho_1=965\pm0.2\%\,\text{kg m}^{-1}$. No surfactants are used. Thus, our study explores three values $\beta=0.2$, 0.05, and 0.01, with $\alpha=1.033$ (see figure 3).

To compare the experiments with the theory, the diameter of the unperturbed jet radius at the orifice exit R_j is estimated by assuming both liquids to issue at an approximately uniform velocity $V=4(Q_1+Q_2)/(\pi D^2)$, Q_1 and Q_2 being the oil and water flow rates (Re_2 ranges from 262 to 1362): $R_j \simeq (D/2)(Q_1/(Q_1+Q_2))^{1/2}$. Knowing R_j, *Re* and *We* can be calculated. We produced five oil flow rates $Q_1=2$, 5, 10, 25, 50, and $100\,\text{ml h}^{-1}$, using a syringe pump (Harvard Apparatus mod. 4455) with B-D $1\,\text{cm}^3$ plastic syringes ($Q_1=1$ and $2\,\text{ml h}^{-1}$), $5\,\text{cm}^3$ ($Q_1=10\,\text{ml h}^{-1}$) and $20\,\text{cm}^3$ ($Q_1=25$ and $50\,\text{ml h}^{-1}$). Two water flow rates $Q_2=1.82$ and $5.16\,\text{ml min}^{-1}$ ($\pm0.5\%$) were supplied, using a pressurized $300\,\text{cm}^3$ water reservoir.

Figure 4 summarizes our experimental results. Note that the J–D transition in flow focusing exhibits a significant hysteresis effect, i.e. parametrical ranges where

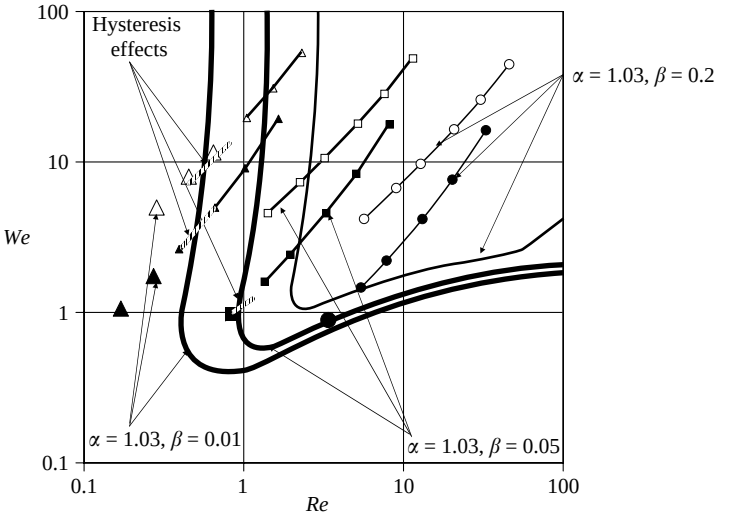

FIGURE 3. Theoretical J–D transition, for various (α, β, Re, We). The lines with symbols show the experiments in figure 4 (small, joined symbols: jetting; isolated large symbols: dripping); $Q_2 = 5.16\,\mathrm{ml\,min^{-1}}$ (open symbols) and $1.82\,\mathrm{ml\,min^{-1}}$ (filled symbols).

(depending on the route followed) meta-stable dripping or jetting may occur in regions corresponding to jetting or dripping, respectively. Hysteresis is caused by the global stability of the system consisting of the capillary feeding tube, the funnel-like meniscus attached to it, and the issuing jet. When the steady jetting regime is left and the dripping regime entered, a considerable part of the apex region (at times, the whole meniscus) oscillates, thus precluding the immediate recovery of steady jet flow conditions, even after the operational parameters return to their original setup in the former jetting regime. To enforce the recovery of jetting conditions, the system must be turned back sufficiently far into the convectively unstable (jetting) parametrical subspace. The amplitude of the hysteretic effect is associated to the meniscus size, i.e. to the relation between feed tube size and orifice diameter: the smaller the feed tube, the smaller the J–D hysteresis, and vice versa. This is entirely analogous to the J–D transition in electrospray, a phenomenon sharing many fundamental features with flow focusing. Moreover, the higher the liquid viscosity, the larger the associated hysteresis effect. In our experiments, we have chosen a sharp-edged (figure 1) feed tube whose inner diameter D_1 coincides with the orifice diameter. We thus minimize the hysteresis effect while maintaining a genuine flow-focusing geometry. Figure 4 shows, whenever it is feasible, the hysteresis range of each experimental sequence.

Therefore, our experiments go from jetting to dripping and not the other way round, because the re-stabilization of a dripping mode requires driving the system very deep inside the jetting mode. Note in figure 4 that, owing to setup limitations, only four of the six experimental sequences were brought into the dripping regime.

Figures 2(*b*) and 3 show a surprising J–D transition topology: the upper branch is slanted so that a potential for double transition exists; should we move along a constant-Re line, we would first meet the J–D transition and subsequently cross a D-J transition. Of course, such a result is to be taken cautiously, because of hysteresis. The potential for double transition is mostly theoretical, since experiments do not follow a constant-Reynolds-number route: when we gradually increase the axial speed V, both the Weber and Reynolds numbers grow (see (2.1)), so that we would move over

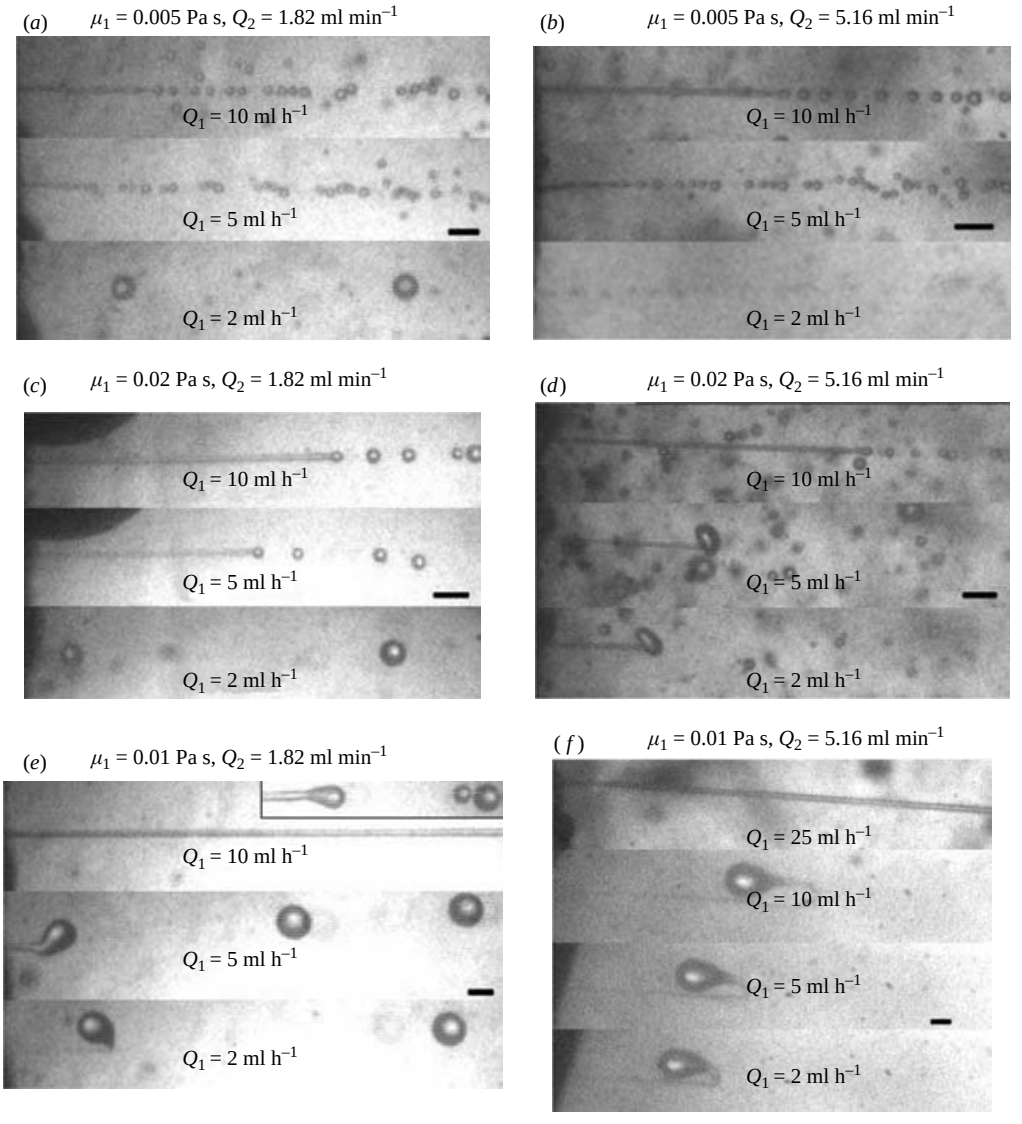

FIGURE 4. Experiments for various values of Q_1, Q_2 and μ_1 ($\alpha = 1.033$; (a, b) $\beta = 0.01$; (c, d) $\beta = 0.05$; (e, f) $\beta = 0.2$; exposure time: 100 ns). The scale is given by the dash, measuring 200 μm. In (e) the insert shows the jet breakup region.

a parabolic line crossing the J–D boundary just once. Another intrinsic experimental difficulty is the water ambient, whose divergent flow after the orifice exit tends to open up the core stream leading to radial dispersal of the drops. Our choice of a sufficiently large L distance ($L = 160\,\mu\text{m} > D$) helps to preserve parallel flow conditions over a distance long enough to give rise to a roughly cylindrical oil jet.

In spite of experimental difficulties, our theoretical model provides a tolerable fit of the J–D transition data as illustrated by the pictures in figure 4. Experimental dot curves in figure 3 show a sequence of five measurements with different core liquid flow rates Q_1; the remaining physical parameters are fixed. The J–D transition takes place at the lowest Q_1 flow rate compatible with a steady jet. Any flow rate

below this threshold produces the emission of large, isolated drops (dripping): the drop-producing mechanism is the sequential filling and detachment from a pulsating axial filament, an elongated version of faucet-dripping (see figure 4*d*). Jetting drops show a diameter, roughly similar to the jet diameter, while dripping drops are substantially larger. The J–D transition is remarkably well-predicted for the smallest viscosity oil (figure 4*a*) and $Q_2 = 1.82\ \mathrm{ml\,min^{-1}}$: it takes place at $Q_1 \simeq 4.9\ \mathrm{ml\,h^{-1}}$. The transition is also very well-predicted at $\beta = 0.05$ for both Q_2 flow rates. When dealing with the largest viscosity oil (figure 4*e*, *f*), the transition is more difficult to assess, although the experimental results fall very close with the predicted transition within the experimental uncertainties associated with the hysteresis effect. In figure 4(*e*, *f*), the top pictures show jetting behaviour, while the remaining shots illustrate a typical dripping process: a long pulsating tendril is filling a thick drop; some recoil is observed, owing to braking effects from the ambient liquid.

4. Concluding remarks

We attempt to provide detailed insight into a particular instance of local convective–absolute (C/A) instability transition. Our choice, a viscous liquid jet co-flowing with another liquid of lesser viscosity, is relevant as a representative flow-focusing setup, with frequent spray and emulsion-producing applications. The dispersion relation is obtained by revisiting prior results from Funada & Joseph (2002), whose analytic formulation is reworked into a simplified formula and then explored assuming complex frequency and wavenumber. Former C/A studies did not fully include viscous effects or were restricted to simple jets flowing in a vacuum. Some analytical challenges have been overcome, among them the detection of the roots and the discrimination among different branches. The structure of the J–D boundary line in the Weber–Reynolds number plane is shown to exhibit an elbow: absolute instability can be reached by sufficiently depressing either We or Re. In the low-Re limit, even a co-flowing liquid shell with negligible density or viscosity is shown to give rise to absolute instability (dripping) for the whole We-range, a result that shows that the jet-in-a-vacuum model by Leib & Goldstein (1998*a*, *b*) must be used cautiously.

The experimental part sums up a large collection of data, and illustrates the correlation between the C/A transition and the onset of dripping. Unwanted effects arising at the nozzle meniscus (a source of independent instability) and an imperfectly cylindrical jet geometry lead to some distortion in the results. Nevertheless, a satisfactory agreement is observed between the breakup pattern sequence and the theoretical prediction.

This work is supported by the Ministry of Science and Technology of Spain, grants nos. DPI2002-04305-C02-02 and DPI2004-07197. Elettra Capozza ran the experiment and took the pictures in her four months stay at our lab, a very appreciated help.

REFERENCES

Ashgriz, N. & Mashayek, F. 1995 Temporal analysis of capillary jet breakup. *J. Fluid Mech.* **291**, 163–190.

Chandrasekhar, S. 1961 *Hydrodynamic and Hydromagnetic Stability*. Dover.

Chomaz, J. M. 2005 Global instabilities in spatially developing flows: Non-normality and nonlinearity. *Annu. Rev. Fluid Mech.* **383**, 357–392.

Clanet, C. & Lasheras, J. C. 1999 Transition from dripping to jetting. *J. Fluid Mech.* **383**, 307–326.

Coullet, P., Mahadevan, L. & Riera, C. S. 2005 Hydrodynamical models for the chaotic dripping faucet. *J. Fluid Mech.* **526**, 1–17.

Cramer, C., Fischer, P. & Windhab, E. J. 2004 Drop formation in a co-flowing ambient fluid. *Chem. Engng Sci.* **59**, 3045–3058.

Funada, T. & Joseph, D. D. 2002 Viscous potential flow analysis of capillary instability. *Intl J. Multiphase Flow* **28**, 1459–1478.

Funada, T., Joseph, D. D. & Yamashita, S. 2004 Stability of a liquid jet into incompressible gases and liquids. *Intl J. Multiphase Flow* **30**, 1279–1310.

Garstecki, P., Fuerstman, M. J. & Whitesides, G. M. 2005 Nonlinear dynamics of a flow-focusing bubble generator: An inverted dripping faucet. *Phys. Rev. Lett.* **94**, 234502.

Huerre, P. & Monkewitz, P. A. 1990 Local and global instabilities in spatially developing flows. *Annu. Rev. Fluid Mech.* **22**, 473–537.

Keller, J. B., Rubinow, S. I. & Tu, Y. O. 1973 Spatial instability of a jet. *Phys. Fluids* **16**, 2052–2055.

Le Dizes, S. 1997 Global modes in falling capillary jets. *Eur. J. Mech.* B/*Fluids* **16**, 761–778.

Leib, S. J. & Goldstein, M. E. 1986a Convective and absolute instability of a viscous liquid jet. *Phys. Fluids* **29**, 952–954.

Leib, S. J. & Goldstein, M. E. 1986b The generation of capillary instabilities on a liquid jet. *J. Fluid Mech.* **168**, 479–500.

Lin, S. P. 2003 *Breakup of Liquid Sheets and Jets*. Cambridge University Press.

Lin, S. P. & Lian, Z. W. 1989 Absolute instability of a liquid jet in a gas. *Phys. Fluids* **31**, 3260–3265.

Lin, S. P. & Lian, Z. W. 1993 Absolute and convective instability of a viscous liquid jet surrounded by a viscous gas in a vertical pipe. *Phys. Fluids* A **5**, 771–773.

Lin, S. P. & Webb, R. 1994 Nonaxisymmetric evanescent waves in a viscous liquid jet. *Phys. Fluids* **6**, 2545–2547.

Monkewitz, P. A. 1990 The role of absolute and convective instability in predicting the behavior of fluid systems. *Eur. J. Mech.* B/*Fluids* **9**, 395–413.

Monkewitz, P. A., Davis, J., Bojorquez, B. & Yu, M. H. 1988 The breakup of a liquid jet at high weber number. *Bull. Am. Phys. Soc.* **33**, 2273.

O'Donnell, B., Chen, J. N. & Lin, S. P. 2001 Transition from convective to absolute instability in a liquid jet. *Phys. of Fluids* **13**, 2732–2734.

Rayleigh, Lord 1878 On the instability of jets. *Proc. Lond. Math. Soc.* **10**, 4–13.

Sevilla, A., Gordillo, J. M. & Martinez-Bazan, C. 2005 Transition from bubbling to jetting in a coaxial air–water jet. *Phys. Fluids* **17**, 018105.

Tomotika, S. 1935 On the instability of a cylindrical thread of a viscous liquid surrounded by another viscous fluid. *Proc. R. Soc. Lond.* A **150**, 322–337.